MNRAS **000**, 1–8 (0000) Preprint 12 May 2023 Compiled using MNRAS LATEX style file v3.0

Detection of the GW of the Crab Pulsar in the LIGO and Virgo O3b series

Herbert Weidner[1] ⋆
[1]*Am Stutz 3, D-63864 Glattbach, Germany*

12 May 2023

ABSTRACT
After compensation for phase modulation and frequency drift, the pulsar's GW can be detected in the records of all three interferometers. The signatures agree with the known values measured with electromagnetic waves.

Key words: Gravitational waves

1 INTRODUCTION

All previous searches for continuous gravitational waves (GW) using different methods have been unsuccessful. This is amazing because the interferometers are extremely sensitive and have recorded large amounts of data. The present study has for the first time succeeded in detecting the gravitational waves of the crab pulsar using standard methods of communications engineering.

This is also due to the fact that the frequency is precisely known from electromagnetic wave observations. Astronomers at the Jodrell Bank Centre for Astrophysics have been observing the pulsar, spinning about 30 times per second. In communications, very weak signals are always received using the same principle: Interfering noise is removed with extremely narrowband filters. The bandwidth of the filter can only be selected to be particularly small if the signal frequency is constant. Unprepared, no GW meets this requirement, as some effects increase the minimum bandwidth:

The Crab pulsar radiates energy and in 2019, the frequency $f_{GW} \approx 59.225$ Hz of the radiation decreases with the velocity $\dot{f}_{pulsar} = -7.37 \times 10^{-10}\ s^{-2}$. One must double the values given in Lyne (1993) because for theoretical reasons $f_{GW} = 2 f_{spin}$ holds.

Since the interferometers rotate once around the axis of the Earth in 24 hours, the Doppler effect produces a small periodic frequency shift of $\Delta f \approx \pm 85\ \mu$Hz (see equation (4)).

Since the pulsar lies close to the plane of the ecliptic, the Doppler effect produces very large periodic frequency changes of about ± 6 mHz because of the high orbital velocity of the Earth around the Sun (about 30 km s^{-1}). This frequency uncertainty can be reduced by choosing special observation periods.

Occasionally and at irregular intervals, the pulsar changes its rotation frequency by several microhertz. Such events are unlikely to interfere if the investigation is limited to a few days.

The prospects of detecting the GW of the Crab pulsar improve if all known modulations are identified and eliminated to reduce the interfering noise by minimizing the signal processing bandwidth.

⋆ E-mail: herbertweidner@gmx.de

2 THE OBSERVATION PERIOD

Every summer the Sun transits the constellation of Taurus, which contains the M1 blast cloud with the central Crab pulsar (ecliptic longitude $\lambda = 84.1^o$, ecliptic latitude $\beta = -1.3^o$). On June 16, Earth - Sun - M1 form almost exactly one line. On this day, the Doppler shift in frequency caused by the high velocity of the Earth as it orbits the Sun is close to zero. Since it is unclear whether the sun influences the propagation of the GW, the following measurements are carried out in a second time window with similar properties: During a short period of a few days around December 16, the frequency change caused by the Earth's orbit is very small and changes proportionally to the time NRAO. Since no sun intervenes between the pulsar and the earth, there is no need to discuss whether and how the sun influences the propagation of GW.

A measurement period of at least 96 hours ensures a sufficient frequency resolution for the following investigation. During this time, the Earth rotates four times around its axis and an interferometer at the prime meridian of the Earth receives twice a day – at midnight and noon – the "true" frequency of the GW generated by the Crab pulsar. At these times, the frequency shift caused by the Doppler effect due to the Earth's rotation disappears. If this instrument had an isotropic antenna sensitivity, it would measure the maximum redshift at 6:00:00 UTC and the maximum blueshift at 18:00:00 UTC.

There is no antenna at this reference point, and for the Hanford, Livingston and Virgo interferometers, the times of the extremes of daily redshift and blueshift are shifted according to their geographic positions. Table 1 shows the expected results for measurements repeating at 24-hour intervals in mid-December.

Each interferometer has a vertical main lobe and is insensitive when the source of the GW is close to the horizon (node of the antenna pattern). But this is the best time period to measure the maximum daily frequency shift (columns 2 and 4 of table 1). Correspondingly, the resulting declination of the GW source can be determined inaccurately.

The opposite is true for the times in columns 3 and 5, because these can be calculated from the zeros of the phase shift ϕ_{day} (see equation (6)). At certain times (column 6) the main lobe of the antenna pattern points approximately into the direction of Crab pulsar and the corresponding interferometer receives a particularly strong

Table 1. Target values of the Doppler shift of the GW of the Crab pulsar on December 16. For other days, the given times shift by −237 seconds per day (sidereal system). The Livingston antenna provides the best signal daily at 6 o'clock (UTC) because its geographic latitude is about the same as the astronomical declination of the Crab pulsar.

Position (–)	Redshift (μHz)	at the time (h UTC)	Blueshift (μHz)	at the time (h UTC)	max. sensitivity (h UTC)
$\lambda = 0^o$, $\varphi = 0^o$	-85	6.0	85	18.0	0
Virgo	-61.5	5.3	61.5	17.3	23.3
Livingston	-73.1	12.05	73.1	0.05	6.05 (good)
Hanford	-58.5	13.96	58.5	1.96	7.96

signal during a short period of time (Figure 9). The Livingston antenna is well positioned with respect to Crab pulsar, but was out of service on 2019 December 16.

When receiving a GW, the position of the Sun does not matter. Therefore, the sidereal daylength of 23.93447192 hours applies in all calculations.

3 SIGNAL PROCESSING

The LIGO interferometers have not yet measured multi-year records, so one must look for the GW of the Crab pulsar in short data series of only a few days duration. This time span is sufficient to measure the periodic frequency shift as a result of the rotation of the Earth.

Data source are the HDF5 files with a sampling frequency of 4096 Hz, which contain strain measurements and supplements for data quality and hardware injections (LIGOdata). No modifications were made because experiments have shown that the use of this information does not improve the S/N in the frequency range around $f_{GW} \approx 60$ Hz. The data reduction is based on the assumption that the frequency of the crab pulsar changes by less than 10 mHz during the measurement period of four weeks. This enables the raw data from the interferometer to be compressed enormously. This happens step by step:

The interferometers deliver data series with very uniform amplitudes around $A \approx 2 \times 10^{-19}$. Significantly high interference peaks ($A > 10^{-17}$) and data gaps are replaced with zero. Further signal processing is based on the software-defined receiver principle.

To display f_{GW} correctly, a sampling frequency > 150 Hz is sufficient. A first decimation by a factor of 20 removes all frequencies above 100 Hz and reduces the file length and calculation time of the subsequent filters.

Because the frequency of the GW is precisely known and occupies a very narrow frequency range, a narrow range around 59.225 Hz is shifted in two steps to $f_{ZF} = 20 \pm 18$ mHz using the heterodydne method. If the frequencies of the local oscillators are constant, these frequency shifts *do not* affect the modulation of the GW. In other words: the signal at f_{ZF} has exactly the same characteristics (drift, phase modulation) as the original signal at f_{GW}. This procedure is modified in section 7.

The low value of f_{ZF} allows decimation by a factor of 160. This reduces the original sampling frequency from 4096 Hz to 0.128 Hz and the file lengths to be processed are reduced by a factor of 32000. A standard laptop is sufficient for processing of the data.

4 THE HETERODYNE METHOD

A central component of all receivers is the mixer, which can shift the signal frequency as required. The main reason used to be (in the age of analogue amplifiers) that low frequencies can be amplified, filtered and shielded more effectively. The frequency of a GW is shifted for other reasons: The modulation frequency $f_{day} \approx 11.6\,\mu$Hz is smaller than f_{GW} by a factor of 5×10^6 and is therefore difficult to detect. If the frequency of the GW is shifted to 0.02 Hz, the modulation frequency can be detected more easily.

The mathematical basis of the frequency shift is the multiplication of two cosine functions.

$$2\cos(\omega_1 t) \cdot \cos(\omega_2 t) = \cos((\omega_1 - \omega_2)t) + \cos((\omega_1 + \omega_2)t) \qquad (1)$$

In digital signal processing, equation 1 is particularly easy to implement, since any computer can multiply two data series element by element:

$\cos(\omega_1 t) = \cos(2\pi t f_{GW})$ is the signal frequency

$\cos(\omega_2 t) = \cos(2\pi t f_{Osz})$ is the local generated auxiliary frequency

$\cos((\omega_1 - \omega_2)t) = \cos(2\pi t f_{ZF})$ is the desired shifted difference frequency

$\cos((\omega_1 + \omega_2)t)$ is undesirable and is suppressed with a low-pass filter.

The heterodyne method is ambiguous because the cos function is axisymmetric: Without special precautions, two different signal frequencies $f_{Osz} + f_{ZF}$ and $f_{Osz} - f_{ZF}$ are received. One of these is desired, the other is called the image frequency and is suppressed by selective filters or by the IQ method.

The locally generated auxiliary frequency f_{Osz} is usually constant, because then the shifted difference frequency f_{ZF} is modulated exactly like the original signal. With the MSH procedure one wants to achieve the opposite: f_{ZF} should be unmodulated. The reasons are explained in section 7.

5 THE SENSITIVITY OF THE INTERFEROMETERS

The S/N determines the quality of the signal reception. The average noise amplitude h_{noise} depends on the inherent noise of the receiver, described by the PSD value, and the bandwidth BW of the receive channel.

$$h_{noise} = \sqrt{PSD \cdot BW} \qquad (2)$$

The LIGO interferometers have PSD values of around 10^{-46} s Biscoveanu (2020); LIGO. One cannot narrow the bandwidth of the signal processing arbitrarily in order to eliminate the disturbing noise.

Because then the necessary time T_{min} that the filter needs to settle down increases. This relationship was first formulated by Küpfmüller and is reminiscent of the Heisenberg uncertainty principle.

$$T_{min} \cdot BW \geq 0.5 \quad (3)$$

The frequency resolution is approximately the reciprocal of the record duration and cannot be improved by changing the sampling frequency. Each record lasts 4096 seconds and limits the spectral resolution to 122 μHz. A comparison of this value with the result of equation (4) shows that one-hour records are too short to detect phase modulation in the diurnal rhythm.

A minimum recording duration 96 hours improves the frequency resolution to 1.5 μHz. Filtering the received data with this bandwidth, the noise floor is as low as $1.2{\times}10^{-26}$ according to equation (2). Since rotating neutron stars are expected to have strains around 10^{-26} Riles (2017), the GW of strong sources should be detectable in the records of the interferometers.

For unknown reasons, the interferometers interrupt the data recording very frequently. This is analogous to digital modulation and creates many and strong sidebands, degrading the S/N of all received signals.

6 PHASE MODULATION OF THE GW

The daily rotation of the interferometers around the earth axis produces a phase modulation with the peak frequency-deviation

$$\Delta f = f_{GW}\left(\sqrt{\frac{v_{GW}+v_{equator}}{v_{GW}-v_{equator}}}-1\right)\cos(\varphi)\cos(\delta) \leq 85\ \mu\text{Hz} \quad (4)$$

The variables mean:
v_{GW} is the propagation velocity of the GW, presumably c
$v_{equator} = 464$ m s^{-1}
φ is the geographic latitude of the interferometer
$\delta = 22^o$ is the declination of the GW source Crab pulsar

Δf cannot be determined directly because the corresponding value is reasonably constant for only a few minutes a day. The short interval does not allow an exact frequency determination (equation 3). The interval length 96 hours is chosen for the search for the GW of the crab pulsar. During this period, the earth spins multiple times and the laws of PM apply. The spectrum of the phase-modulated signal is a bundle of equidistant individual lines with mutual spacing $f_{day} = 11.6$ μHz, filling the Carson bandwidth BW.

$$BW \geq 2(\Delta f + f_{day}) = 193\ \mu\text{Hz} \quad (5)$$

Signal processing with too little bandwidth distorts the PM and prevents decoding. The wide range BW contains the 17 major spectral lines that represent the spectrum of the Crab pulsar, unwanted perturbations, and additional spectral lines produced by other, previously undetected pulsars. The distribution of the total energy of the GW over at least 17 spectral lines lowers the amplitudes and makes it difficult to identify them in the noise and to prove their association. In addition: Our Galaxy probably hosts at least 10^6 pulsars in the frequency range 10 Hz to 200 Hz. The PM in the diurnal rhythm splits each GW into about 30 equidistant spectral lines. It follows that this region is filled with spectral lines whose average spacing is 6 μHz. Sometimes overlaps occur. Figure 1 shows that a spectrum is hardly decipherable, even if it contains only a few phase-modulated signals.

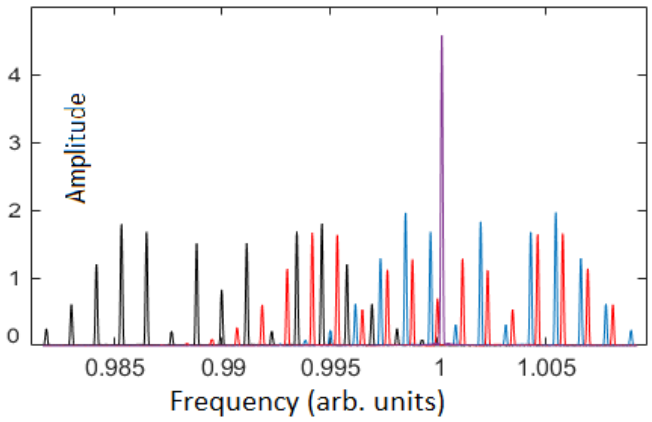

Figure 1. Spectrum of a synthetic data set containing *four* GW with similar frequencies and the same energy. Three GWs are phase modulated in a 24-hour rhythm, one GW is unmodulated. The amplitude of this GW is higher by a factor of three because it is *not* split into 17 sideband frequencies. Noise and drift were omitted because they would cause additional lines. In practice, the spectral lines cannot be assigned based on their color.

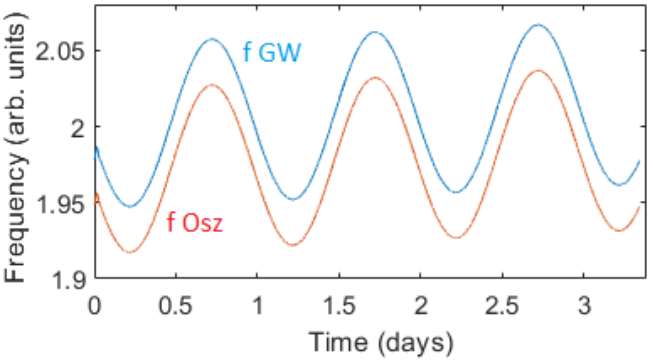

Figure 2. The idea behind the MSH method: The frequency of the GW oscillates around an average value that slowly increases. If one succeeds to generate an auxiliary frequency f_{Osz} with identical modulation, the differential frequency $f_{GW} - f_{Osz}$ (= vertical distance between the two curves) is constant.

7 THE MSH METHOD

A demodulation of the PM with the well-known methods of communications engineering fails due to the poor S/N of the GW and the overlapping of the spectra from different sources. The *Modified SuperHet* (MSH) method avoids any magnitude formation as in Figure 1 and reconstructs a single monochromatic line from phase-related spectral lines *without* the intermediate step of spectral decomposition.

For this purpose, an auxiliary frequency f_{Osz} with a small offset from f_{GW} is generated. The modulation will be changed until the difference frequency is constant (Figure 2). This criterion is easy to monitor and is also suitable for detecting rare frequency jumps (pulsar glitches). Since the difference frequency is unmodulated, it can be processed with an extremely small bandwidth to improve the S/N.

From the 17 spectral lines of a phase-modulated oscillation, the MSH method forms a single one with about three times the amplitude. Illustratively speaking: The many spectral lines inside the

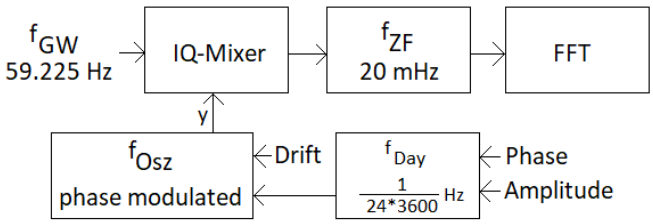

Figure 3. Principle of the MSH method: The parameters for frequency drift and phase modulation of the auxiliary oscillator are iterated until the amplitude of the spectral line at f_{ZF} reaches a maximum. Only a narrow frequency range around f_{ZF} is evaluated (see figure 4). f_{ZF} has no sideband frequencies because the MSH process has removed the modulations from f_{GW}.

bandwidth are rearranged so that they add up to a large total length. The MSH method does not require spectral decomposition of the GW signal as an intermediate step. Neighboring signals are distorted. The advantages of the MSH method:

All lines of a phase modulated GW recombine to a single one and the bandwidth may be reduced from 193 μHz to about 3 μHz. Assuming that the signal processing bandwidth contains only device noise plus a *single* GW, the amplitude of the noise decreases by a factor $a_1 = \sqrt{193/3} \approx 8$. Given the many pulsars in our galaxy, it is questionable whether such wide voids exist.

The MSH process ensures that the energy content of the GW – previously distributed over 17 spectral lines – is now concentrated in the *unmodulated* carrier frequency f_{ZF}. The de-spreading raises the amplitude by a factor of $a_2 \approx 3$.

It is not necessary to identify, measure and recombine of the phases and amplitudes of about 17 spectral lines in the noise. MSH is a coherent detector.

Overall, the amplitude of the single spectral line at f_{ZF} may be $a_1 \cdot a_2 = 24$ times higher than the amplitude of the surrounding noise. Thus, MSH enables the detection and analysis of signals below the noise floor. To my knowledge, no comparable method has ever been used to remove phase modulation from a signal. Details on the use of MSH can be found in Section 11.

8 MATHEMATICAL MODELING

The goal of the investigation is to identify a signal in the records of the LIGO antennas with the properties of the suspected GW of the Crab pulsar. For this purpose, one generates an auxiliary frequency f_{Osz} and iterates its modulation until it agrees in all properties with the suspected GW. The lower part of the figure 3 shows how to create this duplicate. Oscillator-A generates a signal with frequency f_{Osz}, which differs by f_{ZF} from the desired receive frequency f_{GW}. All parameters of this oscillator-A may be controlled, in addition it is phase-modulated by the auxiliary oscillator-B.

The output voltage y from Oscillator-A is used to shift the frequency of the mixed signal supplied by the interferometers to a much lower value f_{ZF}. If oscillator-A is modulated the same as f_{GW}, f_{ZF} is constant and has especially large amplitude because the total energy of the GW is concentrated in a narrow frequency range. The auxiliary oscillation y is generated by the following approach:

$$y = \sin(2\pi t(f_{GW} + f_{ZF} + \dot{f}t + A_{day} \cdot \sin(2\pi t f_{day} + \phi_{day}))) \quad (6)$$

The parameters have the following meaning:

8.1 Frequency of the GW (f_{GW})

We take the initial value of the frequency for 2019 December 15 from the table Lyne (1993) and calculate the initial value for other dates using the nominal value $\dot{f}$. This value is corrected in steps of 3 μHz until we find a high amplitude signal at f_{ZF} that has the expected properties of the GW of the pulsar. There is no peak at f_{GW} in the spectrum. The reason is explained in section 11.

8.2 Intermediate frequency of the MSH method (f_{ZF})

This value is arbitrary, but should be as small as possible so that the daily frequency changes $\Delta f / f_{ZF}$ can be easily seen. Minimum value is the necessary Carson bandwidth BW (equation (5)).

8.3 Frequency drift of GW ($\dot{f}$)

In addition to the inherent frequency drift of the Crab pulsar of $\dot{f}_{pulsar} = -7.365 \times 10^{-10}\ s^{-2}$ Lyne (1993), the Doppler effect produces a time-proportional frequency shift of $\dot{f}_{orbit} = -12.0 \times 10^{-10}\ s^{-2}$ NRAO because of the Earth's orbit. Since these two components cannot be separated experimentally, column 5 of the table 3 contains the measured sum. The nominal value is $\dot{f}_{pulsar} + \dot{f}_{orbit} = -19.365 \times 10^{-10}\ s^{-2}$.

8.4 Modulation index (A_{day})

Because of the Earth's rotation, the frequency of the pulsar changes daily by a maximum of ±85 μHz (equation (4)). One models this variation by a sinusoidal PM. A good starting value for the modulation index of the Crab pulsar is $A_{day} = \Delta f / f_{day} \approx 5$. The geographic latitude of the antenna determines the exact value. Any strong deviation from the expected value indicates that the GW is *not* coming from the direction of the Crab pulsar.

8.5 Modulation frequency (f_{day})

The earth rotates around its axis in 24 hours and a superficial inspection would expect a sinusoidal PM with $f_{day} = 1/24/3600$ Hz. In view of the short records of only 97 hours, a precise indication of the time does not bring any recognizable benefit. The actual rhythm is more complicated, the details are discussed in Section 13.

8.6 Modulation phase (ϕ_{day})

The GW of the Crab pulsar can only be detected with a targeted search because the narrow frequency range around f_{GW} apparently contains several GWs (Figure 7). From the known R.A. of the pulsar follows when the maximum frequency shift of the GW occurs (see table 1). These points in time must remain constant during the iteration in order not to lose sight of the target pulsar. The initial value for ϕ_{day} is calculated from the start time of the analyzed records.

9 FIRST MEASUREMENTS

Can MSH be used to identify the Crab pulsar signal from electromagnetic wave data obtained by the Jodrell Observatory on 2019 December 15? The well-positioned Livingston interferometer was offline on that date, so the test is done with data recorded by the Hanford and Virgo antennas.

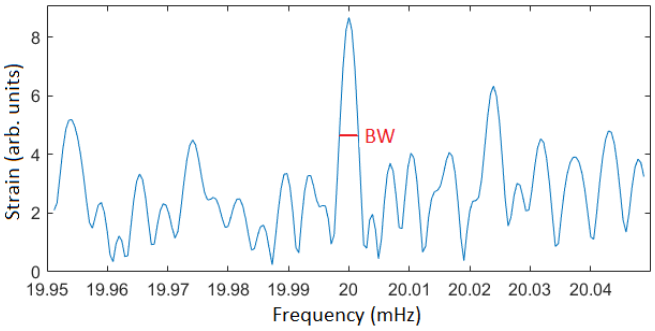

Figure 4. Spectrum of the environment of the GW of the Crab pulsar after removal of the phase modulation and drift and reduction of the frequency to 20 mHz. Source file = V1260445696, recording duration = 97 h. Only the narrow range BW is evaluated, corresponding to a final band-pass filter.

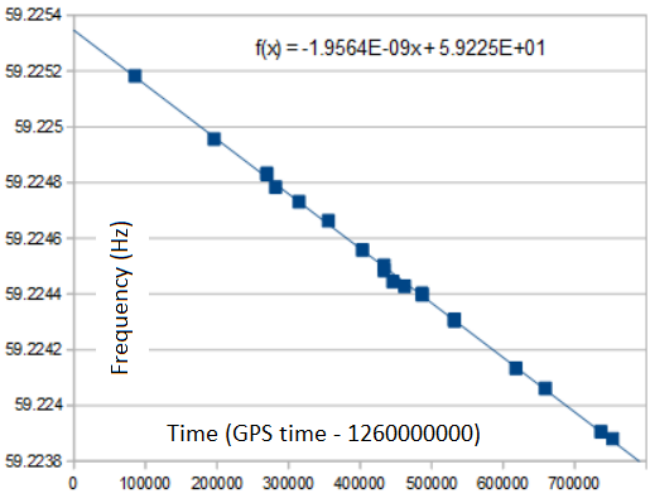

Figure 5. Frequency f_{GW} of the Crab pulsar as a function of time. The dots are the initial frequencies of the 19 data series (see table 3, columns 2 and 3). Each one stretches over a total duration of 97 hours. The start times were chosen so that the total duration contains as few data gaps as possible. The equation at top right is the linear approximation equation.

Figure 4 shows the increase in amplitude after PM and drift are compensated und the entire energy of the Crab pulsar GW is concentrated in a single spectral line. In the spectrum, only the narrow red area at 20 mHz is of interest, containing the modulation-free GW and corresponding to a filter with a bandwidth of 3 μHz. The surrounding area is a mixture of noise and distorted spectra of other GWs, which the interferometer cannot reject because of its low directivity. Some sidebands are caused by the frequent interruptions in the data recordings, acting like a digital modulation.

Result of this measurement: the MSH method shown in figure 3 can remove the PM and the drift of a GW, reduce the bandwidth from 200 μHz (equation (5)) of a signal mixture to 3 μHz, and raise the signal amplitude of the GW by a factor of three.

10 DETAILED MEASUREMENTS IN DECEMBER 2019

The interferometers receive a signal with twice the rotation frequency of the Crab pulsar. To determine the drift and PM properties of this signal, 19 data series with different start dates between 2019 December 11 and 2019 December 19 were formed. Each begins at a precisely defined time and consists of 85 chronologically ordered files, each 4096 seconds long. Gaps and spikes are replaced by zeros. The intial frequency of a data chain is calculated by extrapolation with the nominal value of the drift and corrected iteratively with the MSH method. The actual value of the drift of f_{GW} can be determined in two ways:

One determines the drift of each 97-hour data chain (column 5 in table 3) and averages the individual results $\dot{f}_{orbit} + \dot{f}_{pulsar} = (-18.48 \pm 0.22) \times 10^{-10}\ s^{-2}$. This value is somewhat imprecise due to the short duration of each individual measurement.

One plots the initial frequency of each data chain (column 3 in table 3) as a function of the associated start time (figure 5). The proportionality factor is $\dot{f}_O + \dot{f}_P = -19.56 \times 10^{-10}\ s^{-2}$.

The nominal value of the modulation index $A_{day} = \Delta f / f_{day}$ of the PM depends on the geographical latitude of the antenna (see equation (4). The obtained values (column 4 in table 3) are inaccurate, but close to the nominal values $A_{Livingston} = 6.3$ to $A_{Hanford} = 5.05$. The cause is the unfavorable antenna pattern of the interferometers: Whenever the Doppler effect produces a particularly large frequency shift, the source of the GW lies approximately in the plane defined by the two arms of the interferometer. Then these antennas are particularly insensitive. Interferometers of the present design are not very suitable to determine the declination of the GW source.

11 TECHNICAL DETAILS OF THE MSH PROCESS

The directed search for GW sources is carried out by iterating four parameters of the equation (6). Contrary to all expectations, the value of f_{GW} can only be determined after all other parameters are well known. The cause is the unfavorable value of the modulation index $A_{day} \approx 5.4$, following from equation (4). Because of $J_0(5.52) = 0$ one finds at best a weak spectral line near the expected frequency f_{GW}. Figure 6 shows that the energy of the GW is contained in sidebands surrounding f_{GW}. In view of the bad S/N, it makes little sense to look for the GW in the noise and expect symmetrical spectra. On the one hand, the amplitude distribution is unknown a priori, on the other hand, the numerous sidebands interfere caused by other GWs.

The more precisely the values of drift, modulation index and phase are determined, the higher the amplitude of the central line at f_{ZF} (Figure 4). Then you can correct f_{GW} and end the iteration cycle.

Instructions for use of the MSH method:

One estimates the starting frequency because the spectrum (Figure 6) does not provide any clue for f_{GW}.

With plausible starting values for drift $\dot{f}_{GW}$ and modulation index A_{day}, equation 6 is used to calculate the point in time when the largest frequency deviation Δf can be measured.

The result is often ambiguous (figure 7) and means that there are several pulsars with almost the same frequency, whose GW arrive here from different directions. One decides on a pulsar (here: crab with $\phi_{day} \approx 5$) and narrows the search range of the next iteration steps accordingly.

With the help of equation 6 one optimizes the frequency drift and the modulation index.

The iteration ends when the values of the parameters stabilize after about 10 iterations. Otherwise you shift the starting frequency by about 3 μHz and start a new iteration.

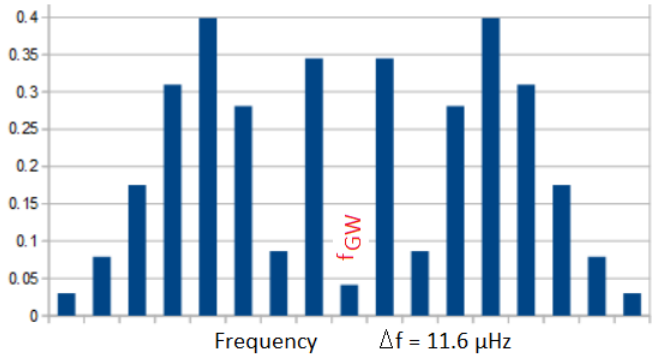

Figure 6. Spectrum of the GW of the crab pulsar with modulation index A_{day} = 5.4 (without drift). The total energy of the GW is distributed over the Carson bandwidth, f_{GW} is barely identifiable. A_{day} determines the individual amplitudes, which are calculated with the Bessel functions $J_n(A_{day})$. Without phase modulation one would see a single spectral line of amplitude $J_0(0) = 1.0$ without sidebands at the central position f_{GW} (n = 0).

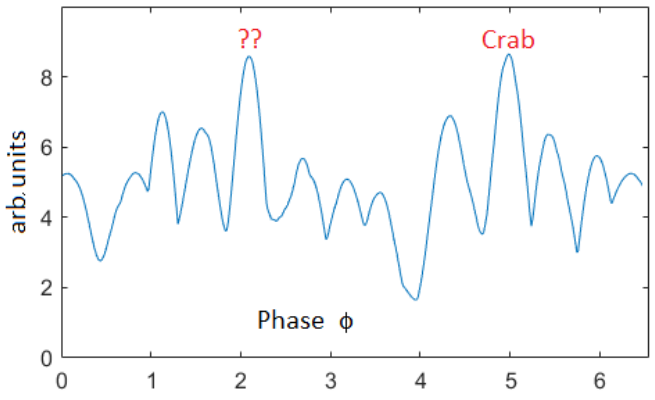

Figure 7. Signal strength as a function of the time of day (see also section 8.6). If you know ϕ_{day} and the start time of the source file V1260445696, you can calculate R.A. of the GW source (see Section 13). Strong maxima mean a GW of the current frequency f_{GW}. The picture shows that there are two strong pulsars of this frequency, whose GW arrive here from almost opposite directions ($\Delta\phi \approx \pi$). The GW with $\phi = 5$ comes from the direction of Crab.

During the iterations one needs to monitor the value of ϕ_{day}. Any deviation means that the GW source changes position. In a way, the dynamics of MSH resemble a phase-locked-loop (PLL) because it keeps centering a phase value once it has been selected.

12 CALCULATION OF THE STRAIN

Einstein feared that GW could never be measured because of its small amplitude. Despite the excellent sensitivity of current antennas (interferometers) in the frequency range around 60 Hz, continuous GW have never been detected using statistical methods. The MSH method described above follows a different path: it bundles the energy of the GW into a single spectral line and thus amplifies it. In order to measure the amplitude, one has to calibrate the vertical scale of figure 4. The *pwelch* function is used to calculate the area under a spectrum peak that exceeds the mean noise level (compare figure 2

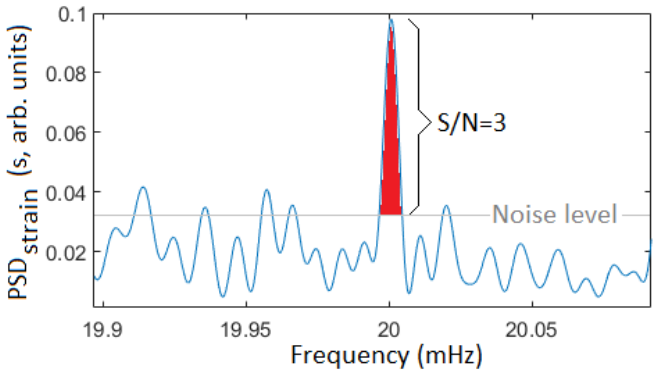

Figure 8. Welch transformation of the spectrum in figure 4. The horizontal line marks the estimated instrument noise level. Because of the short recording duration, f_{GW} does not fit into a single bin of the spectrum. Therefore the red area is a measure for the strain h_{GW}. The reduced noise level compared to figure 4 is a peculiarity of the Welch transform.

in LIGO; Biscoveanu (2020)). The strain h_{GW} is calculated step by step[1]:

The base of the red area in figure 8 is 8.3 μHz wide and corresponds to 17 bins. Each bin is 488 nHz wide.

The noise level reaches the value of 0.033 s, corresponding to $PSD = 10^{-46}$ s of the interferometer.

The summed height of the red area is 0.6304 s (below is just noise). With a significantly longer recording duration, the bandwidth would decrease. Then the GW would fit into a single bin and would have the height $PSD_{GW} = 1.91 \times 10^{-45}$ s.

With equation (2) we get for the strain of the GW:

$$h_{GW}(minimum) = \sqrt{PSD_{GW} \cdot BW} = 3.05 \times 10^{-26} \quad (7)$$

This result agrees well with previous estimates Riles (2017) and is a lower bound. The actual value is probably at least twice as large because the interferometers do not have isotropic directivity. In Abbott (2022), values between 5.5×10^{-26} and 8.79×10^{-26} are specified as the upper limit.

The MSH method hardly reacts to amplitude modulation, but the mean amplitude of the signal decreases (Figur 9).

13 CONTROL MEASUREMENTS

How reliable are the results? How robust is MSH? A strong argument is that the GW of the crab pulsar can be easily detected in *all* datasets from the differently oriented, widely spaced interferometers and almost identical results are obtained for the four parameters of the MSH method (see table 3). The results are insensitive to changes in signal processing parameters such as bandwidth or the initial time of the records.

It might be difficult to measure GW *without* the directional selectivity of the MSH method: Only if f_{GW} and f_{Osc} match very well

[1] The peak should be a few bins wide for sufficient accuracy. This is achieved by zero-padding the data y. In view of the low S/N of the GW, the usual Hann window is replaced by a rectangular window, thus avoiding the loss of information through windowing. In MATLAB, the equivalent statement is: k=16*1024; [sp,f]=pwelch(cat(1,y,zeros(3e5,1)), rectwin(k),k/8,16*k,fs);

in terms of phase and amplitude, the amplitude of f_{ZF} (Figure 2) is high enough for further analysis. As the difference increases, the amplitude drops so much that the MSH method is "blind" for GWs coming from wrong directions (R.A. and declination). An example shows this benefit of directional sensitivity:

The many maxima in figure 7 are a sign that there are several GW sources with almost the same frequency ($f_{GW} \approx 59.22444\ \mu$Hz). Depending on the time of day, the maximum of another GW is measured. Thanks to the directional sensitivity of the MSH method, the sources can be easily distinguished. Table 2 shows the data of the eight strongest GWs in a single file, which can be distinguished by their R.A. Changing the source file to H1260445696 and analyzing again, we get the same data as in table 2 within small tolerances. Further detailed measurements that do not concern the crab pulsar must be omitted here in order not to exceed the scope of this study.

14 THE DIRECTIVITY OF ANTENNAS

The astrophysical waveforms not only present a frequency modulation due to the Doppler shift but also an amplitude modulation. This is due to the fact that interferometeric detectors have non-uniform antenna sensitivity patterns across the sky and the detector response changes in time as the Earth rotates. An interferometer is similar to a fixed zenith/nadir telescope with a narrow field of view.

Although MSH primarily responds to the phase difference between f_{GW} and f_{Osc}, the measurement requires a minimum amplitude of the signal. The analysis shows the core problems: the interferometers distinguish between up and down and are insensitive when the signal source approaches the local horizon. Both influence the evaluation and require a detailed explanation. (In addition, there are frequent data gaps at irregular intervals.)

The following discussion refers to an antenna west of Virgo ($\lambda = 0^o, \varphi = 45^o$). On December 16, the Crab pulsar is south of zenith, the frequency of the GW is *not* Doppler shifted, and the amplitude of the signal is at its maximum. This is the starting position in Figure 9, further points are explained there.

In its simplest form, the MSH method assumes that the antenna is non-directional, receives the signal with approximately constant amplitude throughout the period (97 hours), and that the frequency varies sinusoidally. No interferometer fulfills this ideal. Presumably they receive GW signals in phase opposition from zenith and nadir. Antennas at the equator would provide a cos-shaped normalized amplitude.

These influences ensure that the signals can only be evaluated during certain periods of time. These are shown in Figure 9 as thick blue bars. Their orientation suggests a phase modulation of the GW in a 12-hour rhythm. This question could be checked well with records from the Livingston interferometer, because the latitude of this antenna $\varphi = 31^o$ almost coincides with the declination of the crab pulsar (22^o). Unfortunately, useful data is missing because Livingston was offline in mid-December 2019.

15 DISCUSSION

The crab pulsar's GW is clearly visible in all records ($S/N \approx 3$) and the readings agree very closely with data measured with electromagnetic waves. The amplitude of the crab pulsar's GW (equation 7) corresponds quite closely to the theoretical estimates. There appears to be no offset between the frequency of the EM-observed pulsar rotation and the GW emission process.

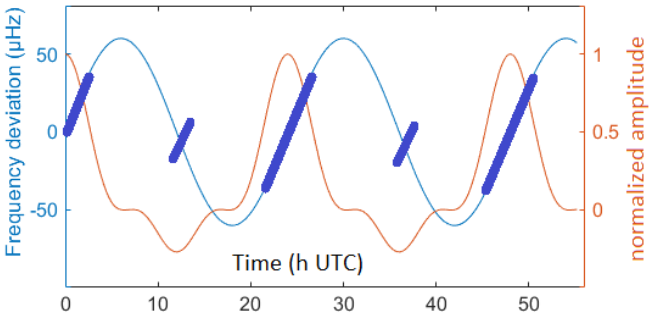

Figure 9. The thin blue sine wave shows the Doppler shift of f_{GW} over two days. The red curve is the putative signal amplitude received by an antenna at $\lambda = 0^o$, $\varphi = 45^o$. At $t = 12$ h and $t = 36$ h, the GW first passes through the earth and then hits the antenna (phase reversal → negative amplitude). Because of the large distance from the perfect position $\lambda = 0^o$, $\varphi = -22^o$ the signal amplitude is quite small. At $t = 6$ h and $t = 18$ h the antenna is insensitive because the GW source is close to the horizon. The meaning of the thick blue bars is explained in the text.

Table 2. Detail measurement of source file V1260445696. In the first step of the MSH procedure one has to decide on a value ϕ_{day} from Fig 7 which is retained during the iteration. MSH determines the values of the other parameters. This file contains the signatures of at least eight pulsars, whose frequencies hardly differ. "Drift" is $\dot{f}_{pulsar} + \dot{f}_{orbit}$. "rel time" is counted from the start time of the file. From this, the R.A. of the GW source can be calculated.

Frequency (Hz)	A_{day} (–)	ϕ_{day} (–)	Drift ($\cdot 10^{-10}\ s^{-2}$)	Ampl. (–)	rel. time (h)
59.2244493522	5.38	0.05	-10.16	10.50	23.56
59.2244484982	3.90	0.99	-18.70	10.00	19.98
59.224444534	5.57	1.01	-25.29	10.00	19.90
59.2244457051	9.28	1.51	-17.93	10.60	18.01
59.2244471514	5.81	2.03	-17.40	9.70	16.03
59.224448715	7.76	4.38	-27.17	8.10	7.08
59.2244452264	7.30	4.98	-18.03	8.65	4.80
59.224453239	6.67	5.17	+10.37	8.60	4.08

Why hasn't the GW of the crab pulsar been identified despite frequent searches? Other search methods differ fundamentally from the MHS method:

5n-vector narrowband pipeline and *Frequency-domain F-statistic pipeline* evaluate short-term spectra. The choice of parameters and the methodology are described in Abbott (2022). What both methods have in common is that they ignore the phases of the GW and – from the point of view of communications engineering – use bandwidths that are considerably too large.

These search methods estimate the sensitivity using a method that is puzzling – at least from a communications engineering perspective: Comparing the formulas $h_{sens} \approx 30\sqrt{PSD/T_{obs}}$ (Abbott (2022), equation (1)) with $h_{noise} = \sqrt{PSD \cdot BW}$ (equation 2), the bandwidth BW of the data processing would have to depend on the observation period T_{obs}. From a communications point of view, this is incomprehensible, everyone uses equation 2.

The empirical formula $h_{sens} \approx 30\sqrt{PSD/T_{obs}}$ is first mentioned

in (Astone (2014), equation (55)) in the context of statistical considerations. Despite an intensive search, I could not find any publication that successfully applies formula (55).

The analysis programs used in Abbott (2022) are sensitive to power supply disturbances (60 Hz in USA). Therefore, an attempt is made to eliminate the interference with a *nonlinear filtering method* that is not described in detail. The MSH method is immune to similar interference because of the narrow bandwidth of the data analysis; non-linear procedures must be avoided because they cause phase distortions and worsen the S/N because they generate unwanted frequencies (intermodulation distortion).

The MSH method has a $processing\ gain \approx 3$ due to the in-phase addition of all sidebands of the PM.

The *5n-vector narrowband pipeline* uses 1024 s long FFTs. According to equation 3, each bin in the spectrum is 488 μHz wide and contains noise of amplitude

$$h_{noise} = \sqrt{PSD \cdot BW} = \sqrt{10^{-46} \cdot 488 \times 10^{-6}} = 2.2 \times 10^{-25} \quad (8)$$

Surprisingly, upper bounds for h_{GW} are calculated between 5.2×10^{-26} and 8.8×10^{-26} (Abbott (2022), Table 2), although the level of h_{GW} is about 10 dB *below* the noise. No methods are described to raise the S/N above the value 1.

When working with the MSH method, one gets the impression that the interferometer records are not unstructured noise, but consist of many GWs with closely spaced frequencies and numerous sidebands. For those GWs, the parameters drift ($\dot{f}_{pulsar} + \dot{f}_{orbit}$) and ecliptic longitude can be determined with surprising accuracy, but not (yet) assigned to any known astronomical object. As soon as the interferometers can measure uninterrupted data series lasting several weeks, the ecliptic latitude of the GW source can also be determined more precisely.

DATA AVAILABILITY

The data underlying this article are available in the Gravitational Wave Open Science Center LIGOdata. All MATLAB programs can be requested from the author.

REFERENCES

Lyne A. et al., 1993, MNRAS, 265, 1003, Jodrell bank crab pulsar monthly ephemeris, https://www.jb.man.ac.uk/pulsar/crab.html

NRAO, Calculate radial velocities, www.gb.nrao.edu/GBT/setups/radvelcalc.html

Biscoveanu S. et al., 2020, Quantifying the Effect of Power Spectral Density Uncertainty on Gravitational-Wave Parameter Estimation, https://arxiv.org/pdf/2004.05149.pdf

Gravitational Wave Open Science Center, O3b Data Release, https://www.gw-openscience.org/data/

Riles K., 2017, Recent searches for continuous Gravitational Waves, Mod. Phys. Lett. A 2017, 32, 1730035, https://arXiv:1712.05897v1

Davis, D. et. al, LIGO Detector Characterization in the Second and Third Observing Runs, https://arxiv.org/pdf/2101.11673.pdf

Abbott, R. et al., Narrowband Searches for Continuous and Long-duration Transient Gravitational Waves from Known Pulsars in the LIGO-Virgo Third Observing Run, The Astrophysical Journal, 932:133 (27pp), 2022

Astone, P. et al., A method for narrow-band searches of continuous gravitational wave signals, Phys. Rev. D 89, 062008, https://arxiv.org/pdf/1403.1484.pdf

This paper has been typeset from a TEX/LATEX file prepared by the author.

Table 3. Single measurements of the GW of the Crab pulsar. The first column gives the location of the antenna; A_{day} is the modulation index of the PM. Column 6 indicates the point in time when the maximum value of the daily frequency shift of the GW is expected; column 7 shows the actual time and column 8 the error.

Location (–)	GPS time (s)	f_{GW} (Hz)	A_{day} (–)	$\dot{f}_O + \dot{f}_P$ $\cdot 10^{-10}\ s^{-2}$	Redshift (h UTC)	Measured at (h UTC)	Error Δt (Minutes)
Livingston	1260085248	59.2251827	2.70	-20.08	12.58	12.61	2.09
Livingston	1260195840	59.2249566	6.83	-17.77	12.45	12.444	-0.12
Virgo	1260269568	59.2248331	4.58	-18.93	5.61	5.605	-0.15
Livingston	1260269568	59.2248295	4.40	-18.43	12.36	12.302	-3.44
Virgo	1260281856	59.2247836	4.71	-17.58	5.59	5.302	-17.49
Hanford	1260314624	59.2247312	4.71	-17.28	14.22	14.185	-1.85
Virgo	1260355584	59.2246634	4.10	-19.37	5.51	5.691	11.08
Hanford	1260433408	59.2245028	4.50	-17.81	14.08	14.366	17.35
Virgo	1260433408	59.2244855	4.20	-17.68	5.42	5.930	30.85
Virgo	1260445696	59.2244452	7.30	-18.03	5.40	4.795	-36.36
Virgo	1260462080	59.2244286	5.18	-18.61	5.38	5.488	6.40
Virgo	1260486656	59.2244024	3.58	-17.65	5.35	5.465	6.71
Hanford	1260486656	59.2243974	5.19	-17.55	14.01	13.778	-14.15
Hanford	1260531712	59.2243040	5.35	-19.49	13.96	14.248	17.19
Virgo	1260531712	59.2243099	2.71	-19.12	5.30	5.268	-1.94
Virgo	1260617728	59.2241339	6.83	-17.26	5.20	4.959	-14.41
Hanford	1260658688	59.2240619	3.59	-20.01	13.81	13.910	5.90
Virgo	1260736512	59.2239060	5.20	-18.73	5.06	5.117	3.45
Livingston	1260752896	59.2238810	7.11	-19.72	11.79	12.081	17.36